

Efficient Mixed-Precision Large Language Model Inference with TurboMind

Li Zhang*
Shanghai AI Laboratory
Shanghai, China
zhangli@pjlab.org.cn

Youhe Jiang*[†]
Shanghai AI Laboratory
Shanghai, China
jiangyouhe@pjlab.org.cn

Guoliang He
Shanghai AI Laboratory
Shanghai, China
heguoliang@pjlab.org.cn

Xin Chen
Shanghai AI Laboratory
Shanghai, China
chenxin@pjlab.org.cn

Han Lv
Shanghai AI Laboratory
Shanghai, China
lvhan@pjlab.org.cn

Qian Yao
Shanghai AI Laboratory
Shanghai, China
yaoqian@pjlab.org.cn

Fangcheng Fu
Shanghai Jiao Tong
University
Shanghai, China
ccchengff@sjtu.edu.cn

Kai Chen
Shanghai AI Laboratory
Shanghai, China
chenkai@pjlab.org.cn

Abstract

Mixed-precision inference techniques reduce the memory and computational demands of Large Language Models (LLMs) by applying hybrid precision formats to model weights, activations, and KV caches. This work introduces mixed-precision LLM inference techniques that encompass (i) systematic memory and compute optimization across hierarchical storage and tensor core architectures, and (ii) comprehensive end-to-end mixed-precision optimization across diverse precision formats and hardware configurations. Our approach features two novel mixed-precision pipelines designed for optimal hardware utilization: a General Matrix Multiply (GEMM) pipeline that optimizes matrix operations through offline weight packing and online acceleration, and an attention pipeline that enables efficient attention computation with arbitrary Query, Key, and Value precision combinations. The key implementation of the pipelines includes (i) hardware-aware weight packing for automatic format optimization, (ii) adaptive head alignment for efficient attention computation, (iii) instruction-level parallelism for memory hierarchy exploitation, and (iv) KV memory loading pipeline for enhanced inference efficiency. We conduct comprehensive evaluations across 16 popular LLMs and 4 representative GPU architectures. Results demonstrate that our approach achieves up to 61% lower serving latency (30% on average) and up to 156% higher throughput (58% on average) in mixed-precision workloads compared to existing mixed-precision frameworks, establishing consistent performance improvements across all tested configurations and hardware types. This work is integrated into TurboMind, a high-performance inference engine of the LMDEPLOY project, which is open-sourced and publicly available at <https://github.com/InternLM/lmdeploy>.

1 Introduction

Large language models (LLMs) such as DeepSeek-R1 [23], OpenAI o3 [58], Claude [7], Gemini [64] and Llama-3 [15] have demonstrated outstanding performance across a wide range of applications (e.g., chatbots, healthcare and education) [22, 27, 60]. However, LLM inference and serving are costly [29, 30, 43], as the large number of model parameters and the generative nature of inference demand substantial memory and compute resources for efficient execution.

Recent efforts [18, 38–40, 71] have explored quantization techniques for efficient LLM inference and serving. Typically, quantization reduces the precision of model weights, activations, and Key-Value (KV) caches from high-precision formats (e.g., FP16, FP32) to lower-precision representations (e.g., INT4, FP8), and carries out the inference process in a mixed-precision manner, significantly reducing memory footprint, memory I/O, and computational overhead [13, 19, 25]. These techniques facilitate more efficient deployment of LLMs while maintaining acceptable model accuracy.

Efficient mixed-precision inference typically requires extensive hardware-specific optimizations for different precision formats, in order to adapt to the multi-layer memory hierarchy and maximize the tensor core utilization of modern hardware. Although recent works have focused on optimizing mixed-precision inference efficiency [14, 19, 39, 56, 61], we identify two fundamental optimization pillars—in which existing frameworks usually fall short—that are essential for delivering high-quality mixed-precision inference.

Pillar 1: Efficient hardware utilization. To achieve efficient LLM inference and serving, it is necessary to make full use of hardware resources of modern GPU architectures, including the memory hierarchy across different levels (e.g., global, shared, and register memory) and compute resources (e.g., arithmetic-logic execution units (ALUs) and tensor cores). However, existing frameworks usually fail to do so. For instance, MARLIN [19], the de facto mixed-precision implementation in vLLM [36], suffers from intrinsic design limitations that prevent it from fully adapting to the memory

*Both authors contributed equally to this research.

[†]This work is done during an internship at Shanghai AI Laboratory.

hierarchy or the tensor core compute capabilities of GPU generations other than Ampere. Similarly, frameworks such as TensorRT-LLM [56] fail to fully leverage the hardware memory hierarchy and incur substantial runtime overhead during dequantization processes [39].

Pillar 2: Holistic mixed-precision optimization. To provision trade-offs between memory/computational efficiency and model accuracy based on user requirements and hardware constraints [18, 38, 71, 74], it necessitates comprehensive support across different precision formats (e.g., varying precision for weights, activations, and KV cache) and operations (e.g., attention and GEMM) based on their specific characteristics. However, existing frameworks typically provide specialized optimizations that both limit their overall optimality and flexibility. For instance, MARLIN [19] provides kernel optimization exclusively for GEMM operations, and thereby computational bottlenecks in non-linear operations (e.g., attention mechanisms) remain and can dominate mixed-precision inference latency. Similarly, QServe [39] is hard-wired to the W4A8KV4¹ precision format, precluding exploration of other precision combinations.

To achieve optimal mixed-precision inference performance, we implement an *efficient* and *holistic* approach in TurboMind, a high-performance inference engine of the LMDEPLOY project. Our key contributions are summarized as follows:

Contribution 1: Bottleneck analysis. We systematically identify and analyze the key memory and compute optimization challenges in typical mixed-precision workflows. These encompass (i) memory access inefficiencies including memory coalescing failures, bank conflicts, and misalignment issues across different hardware memory hierarchies (global memory, shared memory, register memory), as well as (ii) computational bottlenecks including dequantization overhead, suboptimal tensor core utilization, and inefficient attention computation patterns.

Contribution 2: Two optimized pipelines. To address these challenges, we propose two novel mixed-precision implementation pipelines, the *GEMM pipeline* and *attention pipeline*, which provide efficient hardware utilization and comprehensive precision format support for mixed-precision LLM inference. Specifically, (i) the GEMM pipeline resolves the memory and computation inefficiencies across arbitrary precision formats and hardware configurations through an offline weight layout optimization technique, while (ii) the attention pipeline enables arbitrary Query, Key, and Value precision combinations through strategic memory orchestration and meticulous overlapping between computation and memory access.

¹For simplicity, we use “WxAyKVz” to denote the mixed-precision format of x -bit weights, y -bit activations, and z -bit KV caches.

Contribution 3: The thoroughly optimized implementation. Our implementation of the *GEMM pipeline* and *attention pipeline* achieves high efficiency through (i) hardware-aware weight packing for automatic format optimization, (ii) adaptive head alignment to optimize attention memory loading, (iii) instruction-level parallelism for minimizing the dequantization overhead, and (iv) KV memory loading pipeline to enhance attention computation throughput.

Contribution 4: Comprehensive evaluation. We conduct comprehensive evaluations of our mixed-precision workloads across 16 popular LLMs spanning both dense and Mixture-of-Experts (MoE) architectures as well as 4 representative GPU architectures (RTX 4090, L40S, A100, H100), and comparing against existing mixed-precision systems including vLLM enhanced by MARLIN [19, 36, 68, 69], TensorRT-LLM [56], and OmniServe with integrated QServe optimization [39]. Results demonstrate that our system consistently achieves significant performance improvements across all tested configurations, delivering up to 61% lower serving latency (30% on average) and up to 156% higher throughput (58% on average) compared to existing frameworks.

2 Background and Related Works

Memory hierarchy of modern GPUs. Modern GPU architectures feature complex memory hierarchies with distinct performance characteristics that significantly impact LLM inference efficiency. Contemporary GPUs such as the A100 provide multiple memory types including high-bandwidth memory (HBM), L2 cache, shared memory, and register files, each with different latency, bandwidth, and capacity trade-offs [48]. Recent research has explored this hierarchy for LLM workloads [6, 9, 11, 12, 16, 45–47, 75]. FlashAttention [12] and FlashAttention-2 [11] demonstrate substantial improvements through careful orchestration of memory accesses and intermediate result placement; DeepSpeed-Inference [6] and FasterTransformer [46] leverage memory hierarchy awareness for kernel design and data placement strategies; TVM [9] and Ansor [75] enable compiler-level memory hierarchy optimization through automated scheduling; and CUTLASS [47] and cuDNN [45] provide memory-optimized GEMM kernels for different hierarchy levels.

Quantization techniques. Quantization techniques have emerged as essential strategies for reducing the computational and memory demands of LLM inference [18, 24, 32, 38, 40, 71]. Weight quantization approaches such as GPTQ [18], AWQ [38], and SmoothQuant [71] demonstrate that 4-bit and 8-bit model weights can maintain acceptable accuracy while significantly reducing memory footprint. Additionally, KV cache quantization methods focus on compressing the cache during inference. KIVI [40] applies asymmetric 2-bit quantization to KV cache, achieving significant memory reduction while preserving inference quality; ZipCache [24] performs accurate and efficient KV cache quantization with salient

token identification; and GEAR [32] integrates uniform quantization, low-rank matrix approximation, and sparse matrix handling for near-lossless generative inference.

Performance optimization for mixed-precision inference. Recent frameworks aim to improve mixed-precision performance and maximize inference efficiency [19, 39, 39, 56, 61]. MARLIN [19] provides a highly optimized GPU kernel design that enables near-optimal inference performance for quantized LLMs; TensorRT-LLM [56] offers comprehensive mixed-precision optimization through graph-level transformations; QServe [39] introduces novel quantization-aware serving algorithms that co-optimize model compression with system throughput. Recent research also focuses on accelerating low-bit KV cache inference [14, 68]. vLLM [36] implements FP8 KV cache support and specialized attention kernels for reduced precision operations [68]; and BitDecoding [14] targets low-bit KV cache compression to unlock tensor core utilization for long-context LLM decoding scenarios. However, there are two major challenges within current frameworks: (i) They fail to fully exploit the memory hierarchy and tensor core resources of modern hardware. For instance, TensorRT-LLM suffers from significant runtime dequantization overhead with INT4 quantization [39]; (ii) They lack holistic support and optimization for different mixed-precision inference formats. For instance, MARLIN supports GEMM kernel optimization only [19], and QServe is hard-wired to the W4A8KV4 precision format [39].

Our approach. We present an efficient end-to-end optimized solution in §3 for mixed-precision inference that addresses key limitations in existing approaches. Our method (i) integrates memory and compute optimization with explicit consideration of modern GPU memory hierarchy and tensor core utilization within a unified serving architecture, and (ii) introduces dedicated GEMM and attention pipelines that support comprehensive precision combinations of weights, activations, and KV cache (e.g., W4A16KV8). The end-to-end workflow optimization demonstrated in §4 comprises four key technical contributions: (i) hardware-aware weight packing that automatically optimize low-precision weight formats, eliminating manual specifications [19] (§4.1); (ii) adaptive head alignment to enable efficient attention computation without sacrificing memory bandwidth utilization [56, 61] (§4.2); (iii) instruction-level parallelism to fully utilize ALUs and tensor cores instead of naive implementations [56] (§4.3); and (iv) a novel KV memory loading pipeline that further accelerate the inference process (§4.4).

3 Mixed-Precision Inference Pipeline

Mixed-precision inference reduces an LLM’s memory footprint and accelerates memory-bound workloads, by compressing LLM weights to lower bitwidths and dequantizing them on-the-fly. However, enabling efficient mixed-precision

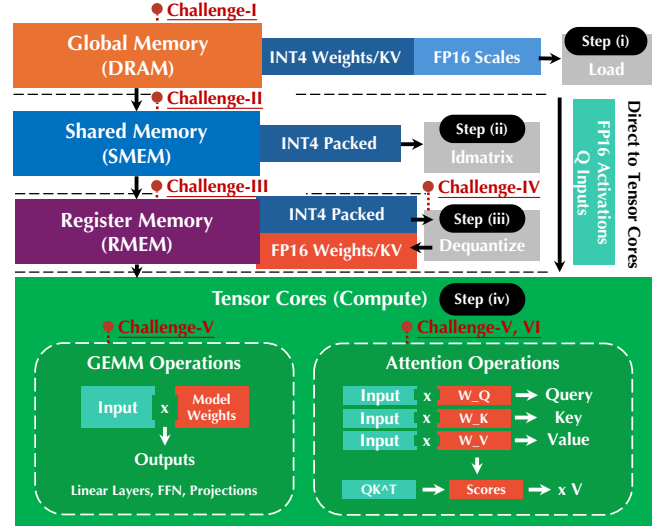


Figure 1. Illustration of the memory hierarchy and each step of the mixed-precision inference workflow.

inference is challenging because it typically demands intensive memory and compute management. In this section, we first introduce a typical mixed-precision inference workflow, then discuss the key challenges in existing pipelines, and finally present our mixed-precision pipeline.

3.1 Typical Mixed-Precision Inference Workflow

Figure 1 illustrates the memory hierarchy and five essential steps in a typical mixed-precision inference workflow with INT4 model weights and KV cache. (i) loading INT4 quantized weights and FP16 scales from global memory into shared memory; (ii) transferring the packed INT4 values to registers using hardware instructions (e.g., `ldmatrix`); (iii) dequantizing the INT4 values to FP16 format through bit manipulation operations, and applying the quantization scales; (iv) feeding the dequantized FP16 weights into tensor cores alongside the FP16 activations to perform standard FP16 matrix multiplication. However, each operation (e.g., memory loading and computation) in the workflow must be carefully managed to achieve efficient implementation.

3.2 Memory Optimization Challenges

It is well known that memory loading can dominate LLM inference, especially during the memory I/O intensive decoding phase, where each decoding step must fetch the full set of model weights, driving arithmetic intensity far below the GPU’s compute-to-bandwidth ratio [2, 59, 77]. Even with aggressive 4-bit compression, weight loads remain the primary bottleneck [19], making further memory optimizations essential for mixed-precision inference. We list the intrinsic memory optimization challenges inherent to each memory layer of the mixed-precision inference workflow as follows.

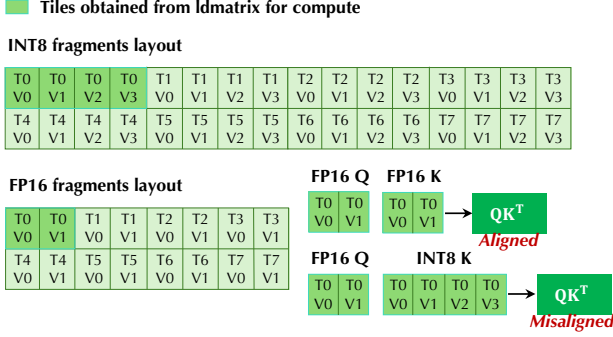


Figure 2. Illustration of register memory misalignment with low-bit KV cache.

Challenge-I: Global memory coalescing. Modern GPUs achieve peak memory bandwidth when the memory addresses accessed by every thread within a warp are within the same aligned segment of global memory (e.g., 3-byte on Hopper/Ampere). This alignment enables the warp to access contiguous memory regions through one efficient global memory transaction [5, 17, 33]. In mixed-precision inference, however, packing weights into low-bit formats results in misalignment between each warp’s memory accesses and the GPU’s standard 32-/64-/128-byte memory segments [53, 54, 70]. This misalignment necessitates multiple global memory transactions per warp for operations rather than one efficient transaction, thereby significantly reducing effective memory bandwidth [18, 34]. An illustration of this process is shown in Appendix B.

Challenge-II: Shared memory bank conflicts. Shared memory bank conflicts occur when multiple threads within a warp simultaneously access different addresses that map to the same memory bank, forcing these accesses to be serialized rather than executed in parallel, thereby reducing memory throughput by up to an order of magnitude [8, 20, 26, 39]. In mixed-precision inference, low-bit values are typically packed into larger-bit words (e.g., eight INT4 values per 32-bit word [57]) to achieve optimal memory bandwidth and space efficiency [19, 56, 61, 63]. However, packing low-bit weights into larger-bit words makes each column load jump a full packed row (e.g., 128-byte for 32 threads read 32-bit words) [53, 54]. That stride maps every thread in the warp to the same shared memory bank, so the bank must serve the requests one-by-one, turning a parallel-access load into a serialized-access stall, severely degrading memory throughput. An illustration of this process is shown in Appendix B.

Challenge-III: Register memory misalignment in low-bit KV cache inference. In mixed-precision inference, compressing the KV cache to low-bit precision (e.g., INT4 or INT8) while leaving the query matrix Q in FP16 creates a byte-stride mismatch: warp-level matrix-load instructions

such as `ldmatrix` fetch wider tiles per lane for K than for Q [14, 55, 67]. The tensor core therefore multiplies misaligned fragments and produces incorrect attention scores in $S = QK^T$, as shown in Figure 2. Current practices mainly disable the warp-level matrix-load instruction to eliminate the layout mismatch. However, this approach requires tensor-core tile reconstruction through additional per-lane address arithmetic and shuffle operations, thereby incurring additional computational overhead and negating most throughput benefits of low-bit KV-cache inference [14, 34, 41].

3.3 Compute Optimization Challenges

Computation overheads in the mixed-precision inference pipeline, e.g., MMA (Matrix Multiply-Accumulate) and dequantization, also have a huge impact on overall performance. We list the computation optimization challenges of the mixed-precision inference workflow as follows.

Challenge-IV: Dequantization overhead. Modern GPUs lack native hardware support for mixed-precision arithmetic between low-bit and FP16 operands, necessitating dequantization before MMA and attention computation [34]. However, naïve type casts from low-bit to FP16 are slow and can become a computational bottleneck [19, 35], making efficient dequantization necessary in mixed-precision inference.

Challenge-V: MMA data misalignment with quantization. Modern tensor cores provide INT8/INT4 MMA instructions, but they only run at full throughput when the inputs are pre-packed into fixed tiles (e.g., $16 \times 8 \times 32/64$ for Ampere, $16 \times 8 \times 64/128$ for Hopper) [1, 42]. Standard quantization layouts seldom meet these hardware requirements, creating a fundamental mismatch between them. Consequently, kernels must either inject padding that wastes compute resources, perform costly in-register shuffles at runtime, or fall back to less efficient scalar operations—all of which erode tensor core throughput [19, 38].

Challenge-VI: Attention computation bubbles. During the decoding phase, each attention head must first load the new key/value rows from the KV cache before the tensor core can start the dot product, causing stall windows since memory traffic and arithmetic execution are serialized rather than overlapped [59, 77]. Quantized KV caches exacerbate this issue: low-bit keys must be fetched and dequantized to FP16 in registers before being consumed by MMA, further extending the stall windows [14, 34]. Thus, the theoretical memory-bandwidth savings from quantization are often negated by the increased bubbles caused by dequantization, yielding negative performance gains in attention-heavy workloads.

3.4 Mixed-Precision Inference Pipeline

To handle the above challenges, we propose two pipelines for GEMM and attention operations, optimizing memory

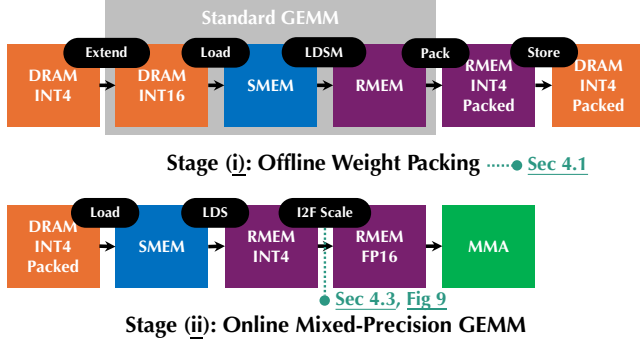


Figure 3. GEMM pipeline. LDSM and LDS are shared memory load instructions for matrix and non-matrix data on Ampere, which can be changed to other specific instructions on other GPU generations.

loading and compute coordination across levels of the memory hierarchy, in order to enhance the system efficiency of mixed-precision LLM inference.

GEMM pipeline. Figure 3 illustrates the INT4 GEMM pipeline. In order to eliminate complex runtime transformations and enable efficient mixed-precision inference, we divide the standard GEMM pipeline into two individual stages: (i) offline low-bit model weight packing and (ii) online mixed-precision GEMM. In the offline weight packing stage, we first extend low-bit weights to 16-bit ones, then load the weight fragments using the same data pipeline as standard GEMM (DRAM→SMEM→RMEM). The fragments are subsequently unextended back to low-bit and stored back to global memory in an optimized format. This offline stage is hardware-aware (detailed in §4.1), converting weight matrices into layouts optimized for efficient memory access and computation without global memory coalescing issues, bank conflicts, or MMA data misalignment issues (**Challenge-I, II, V**). In the online mixed-precision GEMM stage, the pre-processed low-bit fragments are loaded through the standard memory hierarchy, and dequantized into FP16 format through the Integer-to-Float (I2F) procedure for subsequent MMA (**Challenge-IV**). We detailed the dequantization optimization in §4.3. Through offline weight packing, the online stage does not require any additional complex runtime transformations for efficient mixed-precision inference.

Attention pipeline. While leveraging previous memory loading and computation optimizations, our attention pipeline (Figure 4) introduces additional mechanisms tailored for low-bit KV caches. In this pipeline, KV and Q are processed through separate yet coordinated branches. The Q branch applies a shared memory Q rearrangement operation (detailed in §4.2) to resolve register memory misalignment in low-bit KV cache inference (**Challenge-III**), whereas the KV branch loads the low-bit KV cache from global memory, moves it

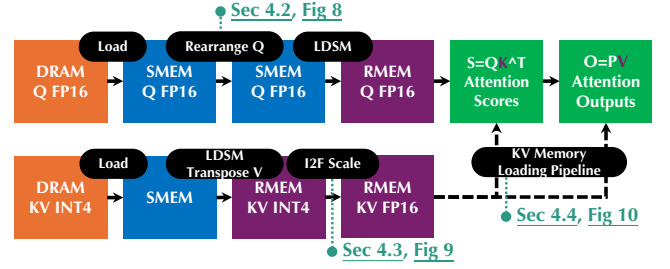


Figure 4. Attention pipeline. The transpose V operation converts V to a column-major tile layout for tensor core compatibility, and the final output O is rearranged back into row-major linear memory before the global write.

through the standard memory hierarchy, and dequantizes it to FP16 using I2F scaling (**Challenge-IV**). Furthermore, the KV memory loading pipeline (detailed in §4.4) overlaps the KV memory loading with dequantization and attention computation, thereby minimizing attention computation bubbles and maintaining high GPU utilization throughout the mechanism (**Challenge-VI**).

4 Implementation

4.1 Hardware-aware Weight Packing

Current weight packing approaches typically employ static weight layout designs that are optimized for specific hardware configurations and tensor core instruction sets. For instance, MARLIN requires manual specifications of optimal configurations including warp layouts and tile sizes, necessitating extensive tuning for different GPU architectures [19]. To address this limitation, we propose a hardware-aware weight packing approach that automatically adapts to different GPU architectures and MMA instruction requirements while maintaining strong performance across diverse hardware configurations. The hardware-aware weight packing process is performed entirely offline.

Hardware-aware weight packing steps. The key insight of our approach is to leverage existing higher precision memory-to-register data pipelines rather than design manual specifications for low-precision formats. During the offline weight packing process, we allow data pipelines to guide the layout transformation, producing packed weights that align perfectly with the hardware’s memory hierarchy and tensor core requirements for efficient online inference. Our approach consists of four essential steps: (i) **Bit extension**. The low-bit weights are temporarily widened to 16-bit format to ensure compatibility with standard (non-mixed-precision) GEMM pipelines. (ii) **Fragment loading**. Each warp issues an asynchronous copy (e.g., cp.async) to move one cache-line-sized slice of the weight matrix (e.g., 128-byte on Ampere [54]) from global to shared memory, then invokes the matrix-load instruction (e.g., LDSM on Ampere) to load the

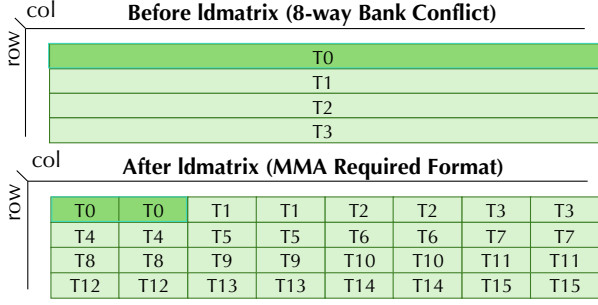


Figure 5. Illustration of matrix-load instructions’ redistribution in step (ii). Before `ldmatrix`, each thread is responsible for loading one matrix row (16-byte), resulting in 8-way bank conflict. This problem is resolved after `ldmatrix`.

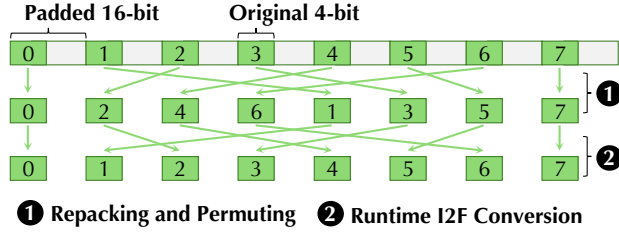


Figure 6. Illustration of repacking and permuting operations in step (iii), and the runtime I2F conversion. The values {0-7} in the figure represent the indices of eight elements within a single thread fragment. This procedure guarantees that, after I2F conversion, the data already match the lane layout required by the MMA instruction.

slice into registers. In this step, the instruction’s internal crossbar automatically redistributes words across lanes [21], as shown in Figure 5. **(iii) Bit compression.** Inside registers, the padded 16-bit words are repacked into their original low-bit format, preserving the lane-level MMA layout established in the previous step, while permuting the sub-word values into the exact order expected by the MMA instruction, as shown in Figure 6. **(iv) Fragment storing.** Each warp writes its packed fragments (typically two at a time for LDS efficiency) back to global memory with a single, fully coalesced cache-line store. As shown in Figure 7, two 16×16 fragments are stored in a flattened $32 \times 2 \times 8$ format. This operation transforms the fragments into a contiguous layout for direct loading, thereby eliminating the additional swizzling operations required during runtime inference. We demonstrate the details of why swizzling operations are required during runtime inference in Appendix C.

Collectively, steps (i)-(iv) pack the model weights into a hardware-optimized layout during the offline process (i.e., hardware-aware weight packing). During the online process (i.e., runtime inference), every warp can reload the weights

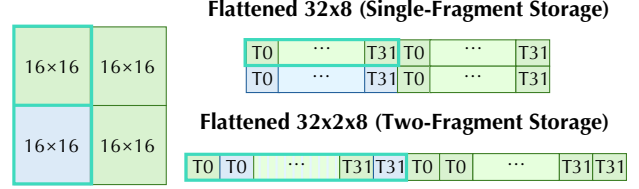


Figure 7. Illustration of fragment storage in step (iv). Single- and two-fragment storage refer to how many packed fragments are written in one store operation. We typically use two-fragment storage for LDS efficiency.

directly and efficiently with the same two-instruction sequence from step (ii): an asynchronous copy followed by the matrix-load instruction (e.g., `cp.async + LDS` on Ampere), without any additional alignment or swizzling overhead. Additionally, this design reduces contention for the ALU units that handle I2F conversions, as fewer arithmetic instructions (e.g., `add`, `multiply`) compete for the same computational resources, improving overall I2F efficiency.

Key advantages. Hardware-aware weight packing achieves broad adaptability across GPU architectures and tensor core generations by leveraging existing data pipelines rather than designing custom layouts. The method provides three built-in performance guarantees: Coalesced global memory transactions (**Challenge-I**), bank-conflict-free shared memory access (**Challenge-II**), and elimination of MMA data misalignment (**Challenge-V**). Consequently, our implementation achieves excellent performance, matching hand-tuned kernels without per-architecture retuning. We evaluate our GEMM kernel performance in §5.2 and examine our GEMM pipeline design across different GPU generations in §5.3 to demonstrate the effectiveness and general applicability of our hardware-aware weight packing approach.

4.2 Adaptive Head Alignment

As discussed in §3.2, mixing FP16 Q with low-bit KV misaligns warp fragments and corrupts $S = QK^T$. Existing frameworks [56, 61, 68] such as PyTorch, TensorRT, and vLLM dequantize the low-bit KV cache back to FP16 before matrix-load instructions to avoid misalignment. However, this extra conversion increases memory traffic and leaves the tensor cores idle, which lowers overall utilization. In contrast to existing works, TurboMind performs a *lightweight* rearrangement of the FP16 Q tensor once per decoding step, aligning its warp-level loads with the low-precision K tiles—thereby delivering satisfactory tensor core throughput without sacrificing utilization.

Rearrange Q. The rearrangement procedure transforms the standard row-major Q layout, aligning FP16 Q fragments with low-precision K fragments for mixed-precision tensor core operations. We adapt Q to different KV precisions in

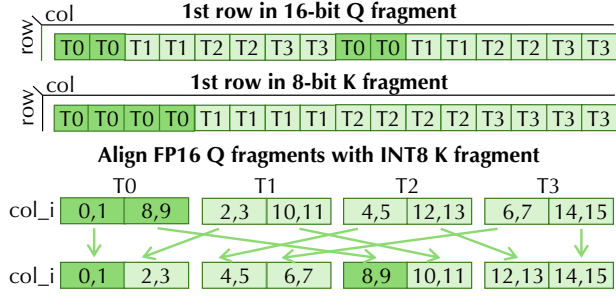


Figure 8. Illustration of aligning FP16 Q with INT8 K fragment. `col_i` represents the column index.

three steps: (i) Computing the appropriate number of K-slices of the Q matrix based on K matrix precision, where K-slices are chunks of the Q matrix along the K dimension. For example, 128-dimensional Q heads require 8, 16, and 32 K-slices for FP16, INT8, and INT4 operands respectively ($OP_K=16, 8, 4$). This step adapts Q slicing to different K matrix precisions for fragment compatibility. (ii) Coordinating thread mapping to Q elements in shared memory access patterns. Each of the 32 threads within a warp computes unique row and column indices to target distinct Q matrix elements. This step ensures conflict-free shared memory bank access during concurrent Q loading. (iii) Employing the LDS instruction to rearrange Q matrix elements into register layouts compatible with tensor cores. The instruction loads Q values from shared memory, and it redistributes them across the 32 threads within a warp (similar to the fragment loading step in §4.1). This step enables efficient tensor core operations without fragment misalignment penalties. We demonstrate the illustration of aligning FP16 Q with INT8 K fragment in Figure 8. We also present the detailed rearrangement pseudocode in Algorithm 1 in Appendix D.

Key advantages. Compared with previous approaches, our adaptive head alignment maximizes hardware utilization by enabling native mixed-precision tensor core operations, and adapts seamlessly to different KV precisions through a single rearrangement procedure. And the Q rearrangement, taking place during shared memory-to-register loading, occurs only once for each attention head, making this approach both computationally efficient and memory-friendly for low-bit KV cache inference (**Challenge-III**). We evaluate the effectiveness of our attention pipeline design in §5.2 and §5.3.

4.3 Instruction-level Parallelism

Simply reading low-bit weights into registers and performing explicit I2F cast is slow, creating a bottleneck in the mixed-precision inference workflow. Thus, we exploit instruction-level parallelism to minimize the dequantization overhead.

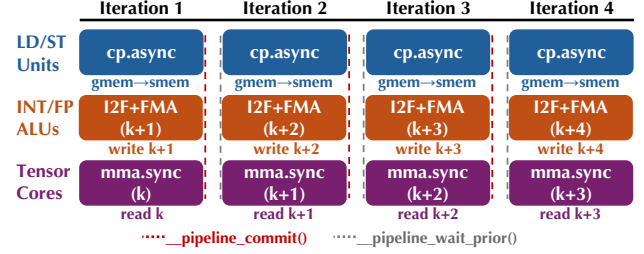


Figure 9. Overall process of parallel MMA-dequantization.

Parallel MMA-dequantization. To minimize the dequantization overhead, we implement a software-pipelined main-loop that orchestrates three concurrent stages across different execution units: (i) Tensor cores execute `mma.sync` operations on the current tile k , performing the matrix multiplication using previously dequantized fragments. (ii) INT/FP ALUs run the I2F conversion and Fused Multiply-Add (FMA) on tile $k+1$ while tensor cores are occupied. (iii) LD/ST (load/store execution) units asynchronously prefetch subsequent tiles² from global memory using `cp.async`, preparing data for future iterations. This three-way overlap is enabled by strategic register allocation, which writes dequantized fragments to registers consumed by the next MMA iteration, eliminating read-after-write hazards. Additionally, CUDA’s asynchronous pipeline primitives (`pipeline_commit` and `pipeline_wait_prior`) manage overlapping `cp.async` operations, ensuring optimal load-compute synchronization throughout the pipeline. We show the overall process of parallel MMA-dequantization in Figure 9.

Key advantages. The instruction-level parallelism optimization can effectively eliminate the dequantization bottleneck (**Challenge-IV**). The parallel MMA-dequantization approach overlaps tensor core computation, I2F conversion and FMA, and `cp.async` operations. This technique enables low-bit matrix multiplication to approach the throughput of pure FP16×FP16 kernels for large-batch inference, while outperforming them at smaller batch sizes, thereby enabling efficient mixed-precision inference across diverse workload scenarios. We perform the evaluation of our instruction-level parallelism in §5.2.

4.4 KV Memory Loading Pipeline

To reduce attention overhead during mixed-precision inference with low-bit KV cache, we implement a pipeline that overlaps memory loading with attention computation, maximizing hardware bandwidth and compute utilization.

Memory loading pipeline for attention computation.

The pipeline overlaps memory loading with computation during the attention computation: K- and V-tiles are loaded

²The number of prefetched tiles is determined by the configured memory pipeline depth, typically ≥ 3 on SM80+ GPU architectures [10].

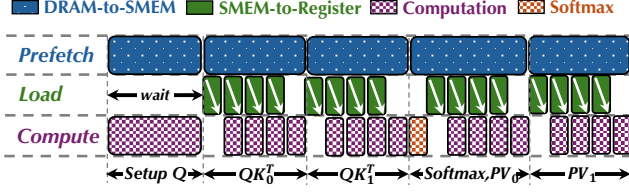


Figure 10. Illustration of the KV memory loading pipeline when the context spans two KV tiles (K_0 , V_0 and K_1 , V_1). The kernel executes the load-compute pipeline in 16-value micro-tiles (a macro-tile consists of 64 tokens) [10].

concurrently with the QK^T and PV computation. For low-bit KV inference, each computation step includes an additional I2F conversion that dequantizes the low-bit KV cache to FP16 format. Such overlap requires triple-level parallelism that simultaneously executes (i) tensor core operations on current data, (ii) shared memory-to-register transfers for upcoming tiles, and (iii) global-to-shared memory prefetching for future pipeline iterations. To enable this coordination, we allocate multi-buffered shared memory to support concurrent data movement across pipeline depths [52].

As shown in Figure 10, our KV memory loading pipeline performs three actions in parallel during attention computation. It concurrently (i) executes the current matrix multiply QK^T/PV on the 16-value slice of the K-/V-tile already in registers, (ii) loads the next 16-value slice of that same tile from shared memory into registers (dequantizing on the fly for a low-bit KV cache), and (iii) prefetches the next K-/V-tile from global to shared memory (this copy starts only when a memory pipeline stage is released). For instance, during QK_0^T computation on the first 16-value slice of K_0 , the second 16-value slice of K_0 is loaded from shared memory to register, and K_1/V_1 are prefetched from global to shared memory, simultaneously. These three overlapping actions keep the pipeline fully occupied, maximizing memory bandwidth utilization and reducing attention computation bubbles.

Key advantages. The memory loading pipeline optimization helps reduce the attention computation bubbles (**Challenge-VI**). It overlaps global-to-shared memory, shared memory-to-register transfers and computations. This technique sustains near-peak HBM bandwidth utilization for attention computation across different KV cache precisions. We demonstrate the performance of our attention kernel in terms of latency and memory bandwidth utilization in §5.2.

5 Evaluation

In this section, we conduct a comprehensive comparison of LMDEPLOY enhanced by TurboMind with state-of-the-art mixed-precision inference and serving frameworks.

5.1 Experiment Setup

Hardware environments. Our experiments are conducted on four different GPU types: RTX 4090 [49], L40S [51], A100 [48], and H100 [50]. For ultra-large LLMs (e.g., Mixtral 8×22B [44], Qwen 235B [72]), we utilize tensor parallelism [66] to accommodate the large model size.

Baselines. We compare LMDEPLOY with other state-of-the-art mixed-precision inference frameworks:

- **vLLM+MARLIN.** vLLM [36] is a state-of-the-art serving framework integrated with MARLIN kernels [19] for mixed-precision LLM inference. We utilize the latest version of vLLM (v0.9.1) for comparison.
- **TensorRT-LLM.** TensorRT-LLM [56] is NVIDIA’s open-source framework for optimizing LLM inference with advanced quantization techniques. We utilize the latest stable release of TensorRT-LLM (v0.20.0) for comparison.
- **OmniServe+QServe.** OmniServe+QServe [39] is a serving system specifically optimized for W4A8KV4 quantization format. We utilize the latest release for comparison.

Models and workloads. Our experiments include models from the Qwen, Llama, DeepSeek, and Mixtral series, spanning different sizes (8B, 32B, 70B, and 235B parameters) and different quantization methods (AWQ [38] and GPTQ [18]). For general conversational tasks, we evaluate these models using real-world chatbot workloads derived from the ShareGPT dataset [65]. For reasoning tasks, we conduct experiments using the reasoning model QwQ [62] on mathematical reasoning workloads from the NuminaMath dataset [4] and the AIMO validation dataset [3]. We follow prior works [30, 37] to generate the inference workload using a Poisson process determined by the request rate.

Evaluation metrics. Following prior works [19, 59, 77], we focus on three primary performance metrics. First, we measure overall system throughput under different inference batch sizes and online serving scenarios. Second, we evaluate system response latency across various percentiles (P50, P90, P95, ..., P99), where P90 latency represents the maximum response time within which 90% of all requests are completed. Third, we report the time-to-first-token (TTFT) latency, the elapsed time between receiving a request and emitting the very first output token, which directly affects perceived responsiveness in interactive applications.

5.2 Kernel Benchmarking

Compare our attention and GEMM kernel performance with vLLM+MARLIN. As shown in Figure 11 and Figure 12, to evaluate the effectiveness of our GEMM and attention pipeline/kernel design in §3.4, we implement a micro-benchmark evaluation on the GEMM and attention kernels using the Qwen 8B AWQ model with 8-bit KV cache (a mixed-precision format of W4A16KV8). We choose vLLM+MARLIN

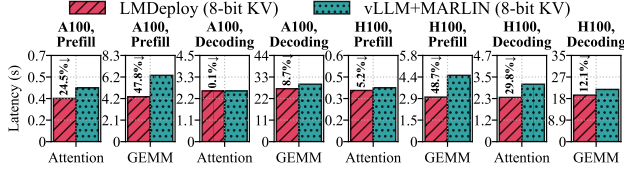


Figure 11. Benchmarking results of prefill and decoding latency for attention and GEMM kernels within a single request on the Qwen3 8B AWQ model with 8-bit KV cache.

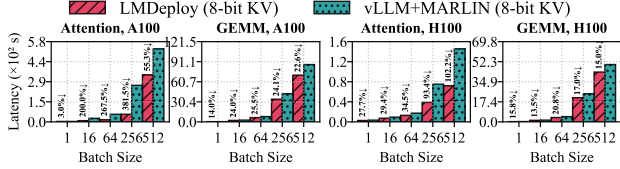


Figure 12. Benchmarking results of accumulated attention and GEMM kernel execution latencies on the Qwen3 8B AWQ model with 8-bit KV cache.

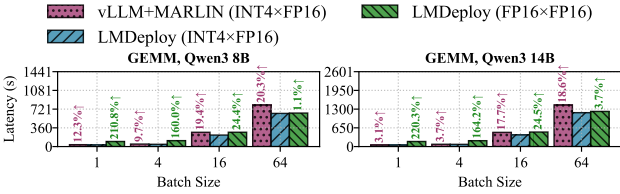


Figure 13. Benchmarking results of our INT4xFP16 kernel versus a general FP16xFP16 GEMM kernel on an A100 GPU.

with 8-bit KV cache compression (fp8_e5m2 [68]) as the baseline method. The results demonstrate that our optimized attention kernel achieves average latency reductions of 22.1% (maximum: 48.7%) during prefill operations and 7.6% (maximum: 29.9%) during decode operations compared with the baseline method, and deliver average latency reductions of 88.5% (maximum: 381.5%) across varying batch sizes, while our optimized GEMM kernels demonstrate average performance gains of 19.2% (maximum: 25.5%) compared to the baseline method. These empirical results substantiate the significance of our GEMM and attention pipeline/kernel design, establishing LMDEPLOY’s superior per-kernel performance relative to the state-of-the-art solution. We also demonstrate the memory bandwidth utilization of LMDEPLOY’s attention kernel in Appendix G. Results show that LMDEPLOY achieves up to 86% and 93% memory bandwidth utilization with 8-bit KV cache, further proving the effectiveness of our attention pipeline design (§3.4).

Compare our mixed-precision GEMM kernel with general GEMM kernel. As illustrated in Figure 13, to evaluate the effectiveness of our instruction-level parallelism mentioned in §4.3, we further compare our INT4xFP16 GEMM

kernel against the general FP16xFP16 GEMM kernel. For small-batch configurations (batch sizes 1-16), our INT4xFP16 kernel achieves an average latency improvement of 134% (maximum 220.3%) over FP16xFP16 implementations. For large-batch scenarios (batch size 64), our INT4xFP16 kernel maintains performance parity with general FP16xFP16 kernels, while the MARLIN mixed-precision kernel suffers up to 20.3% performance degradation. These results validate our instruction-level parallelism design for achieving satisfactory performance during dequantization operations.

We also compare our INT4xFP16 against cuBLAS’s FP16xFP16 GEMM kernel in terms of instruction and cycle counts. The results (detailed in Appendix F) demonstrate that our kernel requires 64.66% more instructions than cuBLAS’s general kernel, primarily due to the additional dequantization operations. However, this instruction overhead translates to only 2.89% more cycles and 2.45% longer execution time, further demonstrating the effectiveness of our instruction-level parallelism in hiding the dequantization latency.

5.3 End-to-end Performance

Compare LMDEPLOY with vLLM+MARLIN. As shown in Figure 14, results show that LMDEPLOY consistently outperforms vLLM+MARLIN [19, 36] across all performance metrics and experimental configurations. We evaluated both systems using Qwen 8B and 32B AWQ models across four different GPU types (RTX 4090, L40, A100, and H100) under varying workload conditions. In terms of throughput, LMDEPLOY achieves an average speedup of 13% compared to vLLM+MARLIN, with a maximum speedup of 31% observed under high-batch scenarios. For TTFT, LMDEPLOY reduces latency by an average of 12.0% (maximum: 33.3%). In online serving scenarios, LMDEPLOY demonstrates superior latency characteristics with an average improvement of 15.0% (maximum: 24.6%) across all latency percentiles (P90-P99). Under varying request arrival rates (1.0 to 10.0 req/s), LMDEPLOY shows even more pronounced benefits, achieving an average latency reduction of 24.1% with maximum improvements of 37.3% at higher request rates. These consistent improvements demonstrate the robustness and general applicability of LMDEPLOY’s mixed-precision inference pipeline (specifically, GEMM pipeline in §3.4). We also compare LMDEPLOY with vLLM in general inference configuration in Appendix H to confirm our performance gains originate from mixed-precision optimization rather than framework differences.

Compare LMDEPLOY with vLLM+MARLIN across a wider range of models. As shown in Figure 15, we conducted an extensive evaluation across 12 diverse models spanning different architectures, parameter scales, and quantization methods. This broader evaluation includes dense models (Llama, Qwen, DeepSeek series) ranging from 7B to 235B parameters, as well as MoE models (Mixtral series), using both AWQ and GPTQ quantization techniques. Across

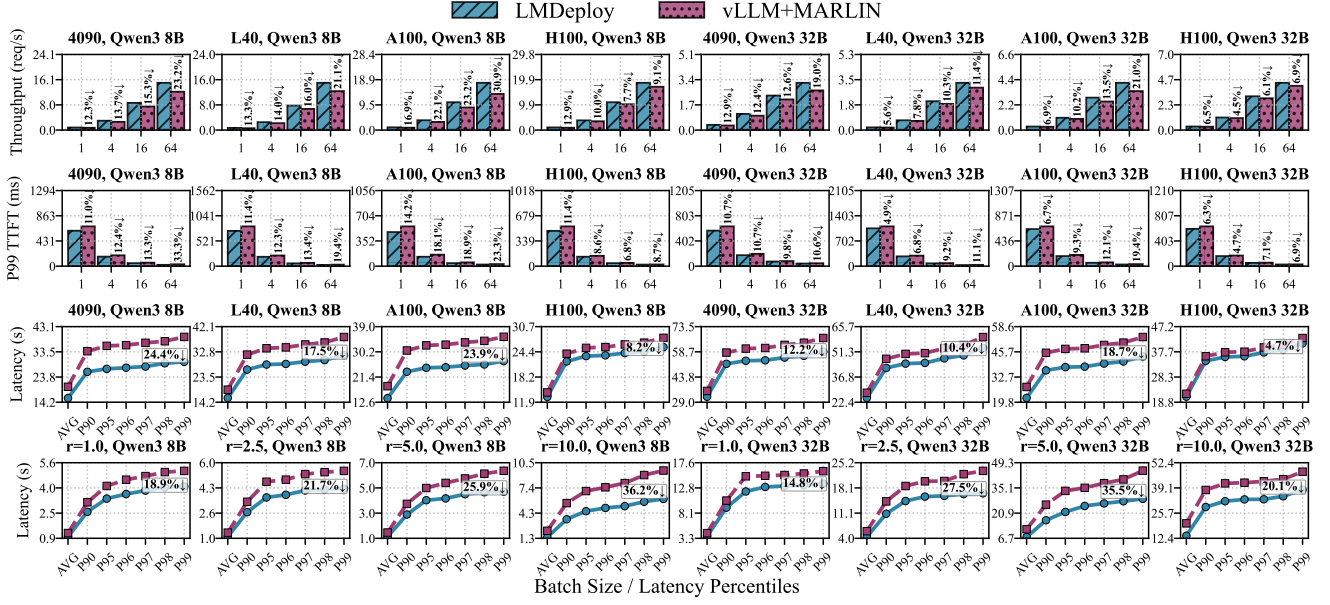


Figure 14. End-to-end experiments comparing LMDEPLOY with vLLM+MARLIN. Rows show: (1-2) throughput and TTFT latency across batch sizes, (3) latency for online serving at maximum batch size and request rate, and (4) latency under varying request rates on A100 GPU.

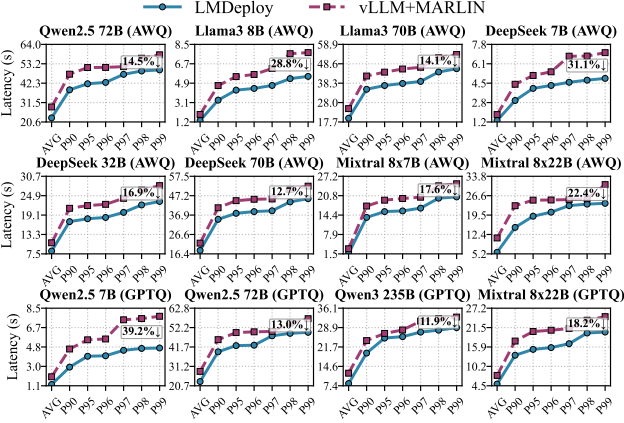


Figure 15. Serving latencies of LMDEPLOY compared with vLLM+MARLIN on different models on A100 GPUs.

this comprehensive model suite, LMDEPLOY achieves an average serving latency improvement of 21.1%, with maximum improvements reaching 47.9%. At the critical P99 latency percentile, LMDEPLOY delivers an average improvement of 20.0% with peak improvements of 39.2%, ensuring reliable performance even under tail latency conditions. These results establish LMDEPLOY as a robust solution for production LLM serving across diverse contemporary LLMs.

Compare LMDEPLOY with vLLM+MARLIN with reasoning models and workloads. As shown in Figure 16, to evaluate LMDEPLOY’s effectiveness on reasoning-intensive

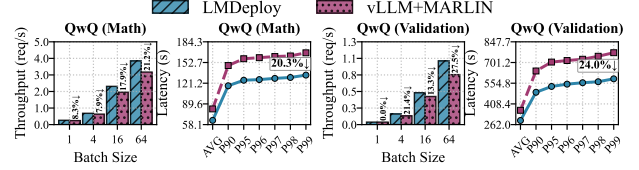


Figure 16. Latency and throughput comparison between LMDEPLOY and vLLM+MARLIN on QwQ with math and validation workloads on an A100 GPU.

workloads, we conducted specialized evaluations using QwQ AWQ models designed for mathematical reasoning and validation tasks. For throughput performance, LMDEPLOY achieves an average speedup of 15% compared to vLLM+MARLIN, with peak improvements of 27% observed in validation tasks. And LMDEPLOY delivers an average latency reduction of 21.9% across all percentiles, with maximum improvements reaching 24.5%. At the critical P99 latency percentile, LMDEPLOY maintains robust performance with 20.3% improvement for mathematical reasoning tasks and 24.0% improvement for validation workloads. These results establish LMDEPLOY’s suitability for sophisticated reasoning tasks.

Compare LMDEPLOY with TensorRT-LLM. As shown in Figure 17, to demonstrate LMDEPLOY’s performance against NVIDIA’s highly optimized inference engine TensorRT-LLM [56], we conducted comparisons using Qwen 7B and 14B AWQ models across multiple evaluation metrics. In throughput performance, LMDEPLOY achieves an average speedup of

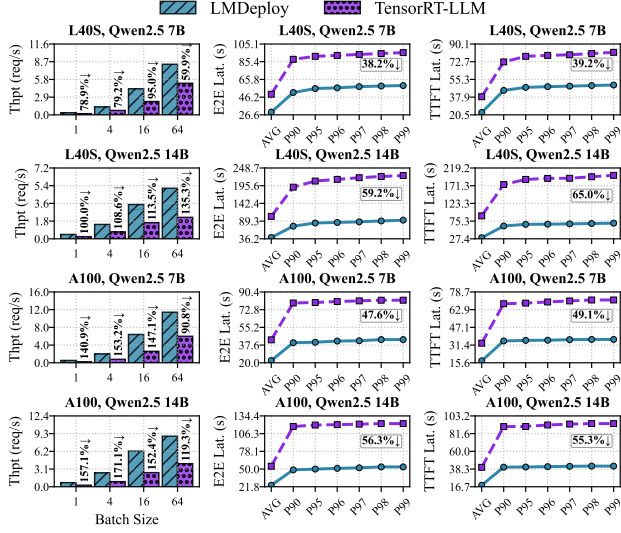


Figure 17. End-to-end experiments of LMDEPLOY compared with TensorRT-LLM on L40S and A100 GPUs.

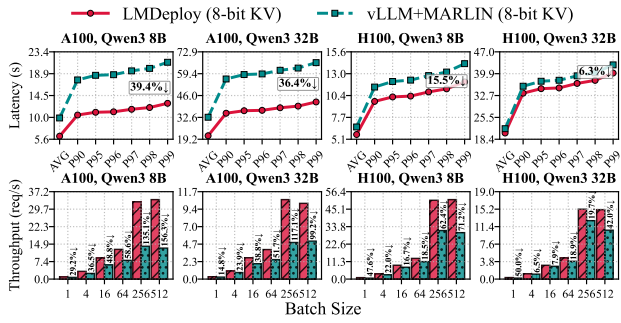


Figure 18. Latency and throughput comparison between LMDEPLOY and vLLM+MARLIN with 8-bit KV cache.

118.90%, with peak speedups reaching 171.11% across different batch configurations. And LMDEPLOY reduces TTFT by an average of 52.2%, with maximum improvements of 65.0%. For end-to-end latency across all percentile measurements, LMDEPLOY delivers an average reduction of 50.3%, with peak improvements of 59.2%. These substantial performance gains further underscore the effectiveness of LMDEPLOY.

Compare LMDEPLOY with vLLM+MARLIN with 8-bit KV cache. As shown in Figure 18, we conducted comprehensive evaluations comparing LMDEPLOY with INT8 KV cache support against vLLM+MARLIN with FP8 KV cache support [68], utilizing Qwen 8B and 32B AWQ models on both A100 and H100 GPUs. For throughput performance, LMDEPLOY achieves an average speedup of 50.6% compared to vLLM+MARLIN, with peak speedups reaching 156.3% in high-batch scenarios on A100 GPUs. And LMDEPLOY reduces latency by an average of 24.6% (maximum: 40.5%) across all percentiles, with P99 latency improving by 24.4% (maximum:

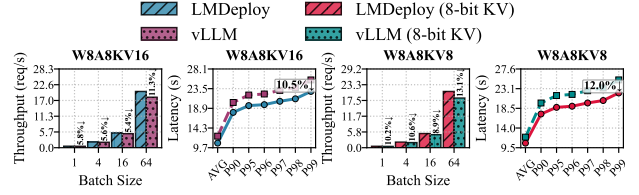


Figure 19. Latency and throughput comparison between LMDEPLOY and vLLM+MARLIN with the FP8 Qwen3 8B model on an H100 GPU.

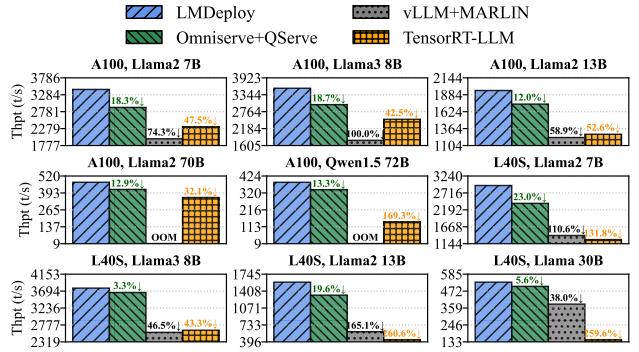


Figure 20. Maximum throughput comparison among LMDEPLOY and baseline frameworks. The experiments follow the benchmarking setting in QServe [39].

39.4%). These results demonstrate the effectiveness of LMDEPLOY’s attention pipeline (§3.4) in low-bit KV cache inference and serving. We also compare the accuracy performance of both frameworks with low-bit KV cache in Appendix E. The results demonstrate the accuracy equivalence.

Compare LMDEPLOY with vLLM on FP8 models. As shown in Figure 19, to further evaluate LMDEPLOY’s effectiveness on FP8 quantized models with different KV cache precision levels, we conducted additional evaluations. Compared with the baseline approach, LMDEPLOY achieves an average performance improvement of 10.4% across both throughput and latency metrics, with peak improvements reaching 13.1%. The consistent performance improvements further demonstrate LMDEPLOY’s comprehensive support for different mixed-precision inference cases.

Compare LMDEPLOY with OmniServe+QServe. As shown in Figure 20, we compare four systems with their optimal precision formats: (i) our system LMDEPLOY (W4A16KV4); (ii) OmniServe+QServe (W4A8KV4) [39], which is a system specifically optimized for W4A8KV4 mixed-precision LLM serving; (iii) vLLM+MARLIN (W4A8KV8); and (iv) TensorRT-LLM (W16A16/W4A16/W8A8KV16), wherein we systematically evaluate the available precision formats across

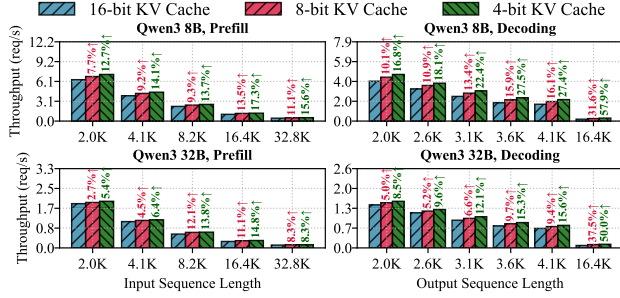


Figure 21. Throughput comparison between different KV precision of LMDEPLOY with different serving batch sizes on an A100 GPU.

different GPU and model configurations and report the optimal variant for each case. LMDEPLOY consistently outperforms all baselines, achieving an average throughput improvement of 14.1% (maximum: 23.0%) over OmniServe-QServe despite the latter’s use of more aggressive 8-bit activation quantization, 84.8% (maximum: 165.1%) over vLLM+M ARLIN, and 115.5% (maximum: 260.6%) over TensorRT-LLM across different GPUs and models. Results show LMDEPLOY’s superior performance even compared to frameworks specifically engineered for certain mixed-precision formats.

5.4 Sensitivity and Scalability

LMDEPLOY performance with different KV cache precisions. As shown in Figure 21, LMDEPLOY demonstrates exceptional performance scalability across different KV cache precision levels. Our comprehensive evaluation across Qwen 8B and 32B AWQ models reveals consistent throughput improvements as KV cache precision is reduced, with benefits observed across both prefill and decoding phases at diverse sequence lengths. When utilizing 8-bit KV cache quantization compared to the 16-bit baseline, LMDEPLOY achieves an average throughput improvement of 11.9%, with peak gains reaching 37.5% in long sequence scenarios. The performance advantages become even more pronounced with aggressive 4-bit KV cache quantization, where LMDEPLOY delivers an average improvement of 18.3% over the 16-bit baseline, with maximum speedups of 57.9% observed in long sequence scenarios. These results demonstrate the efficiency benefits of KV cache compression, while further validating the significance of LMDEPLOY’s attention pipeline design (§3.4). We also demonstrate the scalability of LMDEPLOY with increased tensor parallelism degrees in Appendix I, showing its ability to effectively leverage distributed resources for high-throughput LLM serving.

6 Conclusion

This paper presents the mixed-precision LLM inference and serving techniques integrated in LMDEPLOY that systematically address memory and compute optimization challenges

through novel GEMM and attention pipelines implemented in the TurboMind engine. Our evaluation demonstrates consistent performance improvements, achieving 12-61% lower serving latency with 13-156% higher throughput compared to state-of-the-art mixed-precision frameworks. These results establish LMDEPLOY as an efficient solution for mixed-precision LLM deployment, enabling broader accessibility of LLMs through optimized resource utilization.

References

- [1] 2024. NVIDIA Ampere GPU Architecture Tuning Guide. <https://docs.nvidia.com/cuda/ampere-tuning-guide/index.html>
- [2] Amey Agrawal, Nitin Kedia, Ashish Panwar, Jayashree Mohan, Nipun Kwatra, Bhargav Gulavani, Alexey Tumanov, and Ramachandran Ramjee. 2024. Taming {Throughput-Latency} tradeoff in {LLM} inference with {Sarathi-Serve}. In *18th USENIX Symposium on Operating Systems Design and Implementation (OSDI 24)*. 117–134.
- [3] AI-MO. 2024. AIMO Validation AIME Dataset. <https://huggingface.co/datasets/AI-MO/aimo-validation-aime>
- [4] AI-MO. 2024. NuminaMath-CoT: A Large-Scale Math Dataset with Chain of Thought. <https://huggingface.co/datasets/AI-MO/NuminaMath-CoT>
- [5] Rajeev Alur, Joseph Devietti, Omar S Navarro Leija, and Nimit Singhanian. 2017. GPUDrano: Detecting uncoalesced accesses in GPU programs. In *Computer Aided Verification: 29th International Conference, CAV 2017, Heidelberg, Germany, July 24-28, 2017, Proceedings, Part I 30*. Springer, 507–525.
- [6] Reza Yazdani Aminabadi, Samyam Rajbhandari, Ammar Ahmad Awan, Cheng Li, Du Li, Elton Zheng, Olatunji Ruwase, Shaden Smith, Minjia Zhang, Jeff Rasley, et al. 2022. DeepSpeed-inference: enabling efficient inference of transformer models at unprecedented scale. In *SC22: International Conference for High Performance Computing, Networking, Storage and Analysis*. IEEE, 1–15.
- [7] Anthropic. 2024. The Claude 3 Model Family: Opus, Sonnet, Haiku. https://www-cdn.anthropic.com/de8ba9b01c9ab7cbabf5c33b80b7bbc618857627/Model_Card_Claude_3.pdf
- [8] Girish Biswas and Nandini Mukherjee. 2020. Memory optimized dynamic matrix chain multiplication using shared memory in GPU. In *International Conference on Distributed Computing and Internet Technology*. Springer, 160–172.
- [9] Tianqi Chen, Thierry Moreau, Ziheng Jiang, Lianmin Zheng, Eddie Yan, Haichen Shen, Meghan Cowan, Leyuan Wang, Yuwei Hu, Luis Ceze, et al. 2018. {TVM}: An automated {End-to-End} optimizing compiler for deep learning. In *13th USENIX Symposium on Operating Systems Design and Implementation (OSDI 18)*. 578–594.
- [10] Colfax Research. 2024. CUTLASS Tutorial: Design of a GEMM Kernel. <https://research.colfax-intl.com/cutlass-tutorial-design-of-a-gemm-kernel/>
- [11] Tri Dao. [n. d.]. FlashAttention-2: Faster Attention with Better Parallelism and Work Partitioning. In *The Twelfth International Conference on Learning Representations*.
- [12] Tri Dao, Dan Fu, Stefano Ermon, Atri Rudra, and Christopher Ré. 2022. Flashattention: Fast and memory-efficient exact attention with io-awareness. *Advances in neural information processing systems* 35 (2022), 16344–16359.
- [13] Tim Dettmers, Artidoro Pagnoni, Ari Holtzman, and Luke Zettlemoyer. 2023. Qlora: Efficient finetuning of quantized llms. *Advances in neural information processing systems* 36 (2023), 10088–10115.
- [14] Dayou Du, Shijie Cao, Jianyi Cheng, Ting Cao, and Mao Yang. 2025. BitDecoding: Unlocking Tensor Cores for Long-Context LLMs Decoding with Low-Bit KV Cache. *arXiv preprint arXiv:2503.18773* (2025).

- [15] Abhimanyu Dubey, Abhinav Jauhri, Abhinav Pandey, Abhishek Kadian, Ahmad Al-Dahle, Aiesha Letman, Akhil Mathur, Alan Schelten, Amy Yang, Angela Fan, et al. 2024. The llama 3 herd of models. *arXiv preprint arXiv:2407.21783* (2024).
- [16] Jiarui Fang, Yang Yu, Chengduo Zhao, and Jie Zhou. 2021. Turbotransformers: an efficient gpu serving system for transformer models. In *Proceedings of the 26th ACM SIGPLAN Symposium on Principles and Practice of Parallel Programming*. 389–402.
- [17] Naznin Fauzia, Louis-Noël Pouchet, and P Sadayappan. 2015. Characterizing and enhancing global memory data coalescing on GPUs. In *2015 IEEE/ACM International Symposium on Code Generation and Optimization (CGO)*. IEEE, 12–22.
- [18] Elias Frantar, Saleh Ashkboos, Torsten Hoefer, and Dan Alistarh. 2022. Gptq: Accurate post-training quantization for generative pre-trained transformers. *arXiv preprint arXiv:2210.17323* (2022).
- [19] Elias Frantar, Roberto L Castro, Jiale Chen, Torsten Hoefer, and Dan Alistarh. 2025. Marlin: Mixed-precision auto-regressive parallel inference on large language models. In *Proceedings of the 30th ACM SIGPLAN Annual Symposium on Principles and Practice of Parallel Programming*. 239–251.
- [20] Shuang Gao. 2014. Improving gpu shared memory access efficiency. (2014).
- [21] Mark Gebhart, Stephen W Keckler, Bruce Khailany, Ronny Krashinsky, and William J Dally. 2012. Unifying primary cache, scratch, and register file memories in a throughput processor. In *2012 45th Annual IEEE/ACM International Symposium on Microarchitecture*. IEEE, 96–106.
- [22] GitHub. 2024. The world’s most widely adopted ai developer tool. <https://github.com/features/copilot>
- [23] Daya Guo, Dejian Yang, Haowei Zhang, Junxiao Song, Ruoyu Zhang, Runxin Xu, Qihao Zhu, Shirong Ma, Peiyi Wang, Xiao Bi, et al. 2025. Deepseek-r1: Incentivizing reasoning capability in llms via reinforcement learning. *arXiv preprint arXiv:2501.12948* (2025).
- [24] Yefei He, Luoming Zhang, Weijia Wu, Jing Liu, Hong Zhou, and Bohan Zhuang. [n. d.]. ZipCache: Accurate and Efficient KV Cache Quantization with Salient Token Identification. In *The Thirty-eighth Annual Conference on Neural Information Processing Systems*.
- [25] Coleman Hooper, Sehoon Kim, Hiva Mohammadzadeh, Michael W Mahoney, Yakun S Shao, Kurt Keutzer, and Amir Gholami. 2024. Kvquant: Towards 10 million context length llm inference with kv cache quantization. *Advances in Neural Information Processing Systems* 37 (2024), 1270–1303.
- [26] Adrian Horga, Ahmed Rezine, Sudipta Chattopadhyay, Petru Eles, and Zebo Peng. 2022. Symbolic identification of shared memory based bank conflicts for GPUs. *Journal of Systems Architecture* 127 (2022), 102518.
- [27] Jaeho Jeon and Seongyong Lee. 2023. Large language models in education: A focus on the complementary relationship between human teachers and ChatGPT. *Education and Information Technologies* 28, 12 (2023), 15873–15892.
- [28] YOUHE JIANG, Fangcheng Fu, Xiaozhe Yao, Guoliang HE, Xupeng Miao, Ana Klimovic, Bin CUI, Binhang Yuan, and Eiko Yoneki. 2025. Demystifying Cost-Efficiency in LLM Serving over Heterogeneous GPUs. In *Forty-second International Conference on Machine Learning*.
- [29] YOUHE JIANG, Fangcheng Fu, Xiaozhe Yao, Taiyi Wang, Bin CUI, Ana Klimovic, and Eiko Yoneki. [n. d.]. ThunderServe: High-performance and Cost-efficient LLM Serving in Cloud Environments. In *Eighth Conference on Machine Learning and Systems*.
- [30] Youhe Jiang, Ran Yan, Xiaozhe Yao, Yang Zhou, Beidi Chen, and Binhang Yuan. 2024. HexGen: Generative Inference of Large Language Model over Heterogeneous Environment. In *International Conference on Machine Learning*. PMLR, 21946–21961.
- [31] YOUHE JIANG, Ran Yan, and Binhang Yuan. 2025. HexGen-2: Disaggregated Generative Inference of LLMs in Heterogeneous Environment. In *The Thirteenth International Conference on Learning Representations*.
- [32] Hao Kang, Qingru Zhang, Souvik Kundu, Geonhwa Jeong, Zaoxing Liu, Tushar Krishna, and Tuo Zhao. 2024. Gear: An efficient kv cache compression recipe for near-lossless generative inference of llm. *arXiv preprint arXiv:2403.05527* (2024).
- [33] Dae-Hwan Kim. 2017. Evaluation of the performance of GPU global memory coalescing. *Evaluation* 4, 4 (2017), 1–5.
- [34] Taesu Kim, Jongho Lee, Daehyun Ahn, Sarang Kim, Jiwoong Choi, Minkyu Kim, and Hyungjun Kim. 2024. QUICK: Quantization-aware Interleaving and Conflict-free Kernel for efficient LLM inference. *arXiv preprint arXiv:2402.10076* (2024).
- [35] Young Jin Kim, Rawn Henry, Raffi Fahim, and Hany Hassan Awadalla. 2022. Who Says Elephants Can’t Run: Bringing Large Scale MoE Models into Cloud Scale Production. In *Proceedings of The Third Workshop on Simple and Efficient Natural Language Processing (SustaiNLP)*. 36–43.
- [36] Woosuk Kwon, Zhuohan Li, Siyuan Zhuang, Ying Sheng, Lianmin Zheng, Cody Hao Yu, Joseph Gonzalez, Hao Zhang, and Ion Stoica. 2023. Efficient memory management for large language model serving with pagedattention. In *Proceedings of the 29th Symposium on Operating Systems Principles*. 611–626.
- [37] Zhuohan Li, Lianmin Zheng, Yinmin Zhong, Vincent Liu, Ying Sheng, Xin Jin, Yanping Huang, Zhifeng Chen, Hao Zhang, Joseph E Gonzalez, et al. 2023. {AlpaServe}: Statistical multiplexing with model parallelism for deep learning serving. In *17th USENIX Symposium on Operating Systems Design and Implementation (OSDI 23)*. 663–679.
- [38] Ji Lin, Jiaming Tang, Haotian Tang, Shang Yang, Wei-Ming Chen, Wei-Chen Wang, Guangxuan Xiao, Xingyu Dang, Chuang Gan, and Song Han. 2024. Awq: Activation-aware weight quantization for on-device llm compression and acceleration. *Proceedings of Machine Learning and Systems* 6 (2024), 87–100.
- [39] Yujun Lin, Haotian Tang, Shang Yang, Zhekai Zhang, Guangxuan Xiao, Chuang Gan, and Song Han. 2024. Qserve: W4a8kv4 quantization and system co-design for efficient llm serving. *arXiv preprint arXiv:2405.04532* (2024).
- [40] Zirui Liu, Jiayi Yuan, Hongye Jin, Shaochen Zhong, Zhaozhao Xu, Vladimir Braverman, Beidi Chen, and Xia Hu. 2024. KIVI: A Tuning-Free Asymmetric 2bit Quantization for KV Cache. In *International Conference on Machine Learning*. PMLR, 32332–32344.
- [41] Justin Luitjens. 2025. CUDA Pro Tip: Increase Performance with Vectorized Memory Access. <https://developer.nvidia.com/blog/cuda-pro-tip-increase-performance-with-vectorized-memory-access/>
- [42] Weile Luo, Ruibo Fan, Zeyu Li, Dayou Du, Qiang Wang, and Xiaowen Chu. 2024. Benchmarking and dissecting the nvidia hopper gpu architecture. In *2024 IEEE International Parallel and Distributed Processing Symposium (IPDPS)*. IEEE, 656–667.
- [43] Xupeng Miao, Chunan Shi, Jiangfei Duan, Xiaoli Xi, Dahua Lin, Bin Cui, and Zhihao Jia. 2024. Spotserve: Serving generative large language models on preemptible instances. In *Proceedings of the 29th ACM International Conference on Architectural Support for Programming Languages and Operating Systems, Volume 2*. 1112–1127.
- [44] Mistral AI. 2024. Mixtral 8x22B: Cheaper, Better, Faster, Stronger. <https://mistral.ai/news/mixtral-8x22b>
- [45] NVIDIA Corporation. 2014. cuDNN: NVIDIA CUDA Deep Neural Network Library. <https://developer.nvidia.com/cudnn>
- [46] NVIDIA Corporation. 2019. FasterTransformer: Transformer related optimization, including BERT, GPT. <https://github.com/NVIDIA/FasterTransformer>
- [47] NVIDIA Corporation. 2020. CUTLASS: CUDA Templates for Linear Algebra Subroutines. <https://github.com/NVIDIA/cutlass>

- [48] NVIDIA Corporation. 2020. NVIDIA A100 Tensor Core GPU Architecture. <https://www.nvidia.com/en-us/data-center/a100/>
- [49] NVIDIA Corporation. 2022. NVIDIA GeForce RTX 4090 Graphics Card. <https://www.nvidia.com/en-us/geforce/graphics-cards/40-series/rtx-4090/>
- [50] NVIDIA Corporation. 2022. NVIDIA H100 Tensor Core GPU Architecture. <https://www.nvidia.com/en-us/data-center/h100/>
- [51] NVIDIA Corporation. 2023. NVIDIA L40S Data Center GPU. <https://www.nvidia.com/en-us/data-center/l40s/>
- [52] NVIDIA Corporation. 2024. Efficient GEMM in CUDA. https://github.com/NVIDIA/cutlass/blob/main/media/docs/efficient_gemm.md
- [53] NVIDIA Corporation. 2024. NVIDIA TensorRT 10.0.1 Developer Guide. <https://docs.nvidia.com/deeplearning/tensorrt/archives/tensorrt-1001/developer-guide/index.html>
- [54] NVIDIA Corporation. 2025. CUDA C++ Programming Guide, Release 12.9. <https://docs.nvidia.com/cuda/cuda-c-programming-guide/>
- [55] NVIDIA Corporation. 2025. Parallel Thread Execution (PTX) ISA: 1dmatrix Instruction. <https://docs.nvidia.com/cuda/parallel-thread-execution/>
- [56] NVIDIA Corporation. 2025. TensorRT-LLM. <https://github.com/NVIDIA/TensorRT-LLM>
- [57] NVIDIA Corporation. 2025. Working with Quantized Types. <https://docs.nvidia.com/deeplearning/tensorrt/latest/inference-library/work-quantized-types.html>
- [58] OpenAI. 2025. OpenAI o3. <https://platform.openai.com/docs/models/o3>
- [59] Pratyush Patel, Esha Choukse, Chaojie Zhang, Aashaka Shah, Íñigo Goiri, Saeed Maleki, and Ricardo Bianchini. 2024. Splitwise: Efficient generative llm inference using phase splitting. In *2024 ACM/IEEE 51st Annual International Symposium on Computer Architecture (ISCA)*. IEEE, 118–132.
- [60] Cheng Peng, Xi Yang, Aokun Chen, Kaleb E Smith, Nima PourNejatian, Anthony B Costa, Cheryl Martin, Mona G Flores, Ying Zhang, Tanja Magoc, et al. 2023. A study of generative large language model for medical research and healthcare. *NPJ digital medicine* 6, 1 (2023), 210.
- [61] PyTorch Core Team. 2025. PyTorch. <https://pytorch.org>
- [62] Qwen Team. 2025. QwQ-32B: Embracing the Power of Reinforcement Learning. <https://qwenlm.github.io/blog/qwq-32b/>
- [63] Mariam Rakka, Mohammed E Fouda, Pramod Khargonekar, and Fadi Kurdahi. 2022. Mixed-precision neural networks: A survey. *arXiv preprint arXiv:2208.06064* (2022).
- [64] Machel Reid, Nikolay Savinov, Denis Teplyashin, Dmitry Lepikhin, Timothy Lillicrap, Jean-baptiste Alayrac, Radu Soricut, Angeliki Lazariidou, Orhan Firat, Julian Schrittwieser, et al. 2024. Gemini 1.5: Unlocking multimodal understanding across millions of tokens of context. *arXiv preprint arXiv:2403.05530* (2024).
- [65] ShareGPT Team. 2023. ShareGPT: Share your wildest ChatGPT conversations with one click. <https://sharegpt.com/>
- [66] Mohammad Shoeybi, Mostofa Patwary, Raul Puri, Patrick LeGresley, Jared Casper, and Bryan Catanzaro. 2019. Megatron-lm: Training multi-billion parameter language models using model parallelism. *arXiv preprint arXiv:1909.08053* (2019).
- [67] Yifan Tan, Haoze Wang, Chao Yan, and Yangdong Deng. 2024. AlignedKV: Reducing Memory Access of KV-Cache with Precision-Aligned Quantization. *arXiv preprint arXiv:2409.16546* (2024).
- [68] vLLM Team. 2024. Quantized KV Cache. https://docs.vllm.ai/en/stable/features/quantization/quantized_kvcache.html
- [69] vLLM Team. 2024. vLLM Quantization: Supported Hardware. https://docs.vllm.ai/en/latest/features/quantization/supported_hardware.html
- [70] Wright, Less and Hoque, Adnan. 2024. Accelerating Triton Dequantization Kernels for GPTQ. <https://pytorch.org/blog/accelerating-triton/>
- [71] Guangxuan Xiao, Ji Lin, Mickael Seznec, Hao Wu, Julien Demouth, and Song Han. 2023. Smoothquant: Accurate and efficient post-training quantization for large language models. In *International Conference on Machine Learning*. PMLR, 38087–38099.
- [72] An Yang, Anfeng Li, Baosong Yang, Beichen Zhang, Binyuan Hui, Bo Zheng, Bowen Yu, Chang Gao, Chengen Huang, Chenxu Lv, et al. 2025. Qwen3 technical report. *arXiv preprint arXiv:2505.09388* (2025).
- [73] Gyeong-In Yu, Joo Seong Jeong, Geon-Woo Kim, Soojeong Kim, and Byung-Gon Chun. 2022. Orca: A distributed serving system for {Transformer-Based} generative models. In *16th USENIX Symposium on Operating Systems Design and Implementation (OSDI 22)*. 521–538.
- [74] Yilong Zhao, Chien-Yu Lin, Kan Zhu, Zihao Ye, Lequn Chen, Size Zheng, Luis Ceze, Arvind Krishnamurthy, Tianqi Chen, and Baris Kasicki. 2024. Atom: Low-bit quantization for efficient and accurate llm serving. *Proceedings of Machine Learning and Systems* 6 (2024), 196–209.
- [75] Lianmin Zheng, Chengfan Jia, Minmin Sun, Zhao Wu, Cody Hao Yu, Ameer Haj-Ali, Yida Wang, Jun Yang, Danyang Zhuo, Koushik Sen, et al. 2020. Ansor: Generating {High-Performance} tensor programs for deep learning. In *14th USENIX symposium on operating systems design and implementation (OSDI 20)*. 863–879.
- [76] Lianmin Zheng, Liangsheng Yin, Zhiqiang Xie, Chuyue Livia Sun, Jeff Huang, Cody Hao Yu, Shiyi Cao, Christos Kozyrakis, Ion Stoica, Joseph E Gonzalez, et al. 2024. Sglang: Efficient execution of structured language model programs. *Advances in Neural Information Processing Systems* 37 (2024), 62557–62583.
- [77] Yinmin Zhong, Shengyu Liu, Junda Chen, Jianbo Hu, Yibo Zhu, Xuanzhe Liu, Xin Jin, and Hao Zhang. 2024. {DistServe}: Disaggregating prefill and decoding for goodput-optimized large language model serving. In *18th USENIX Symposium on Operating Systems Design and Implementation (OSDI 24)*. 193–210.

A Extended Related Works

LLM inference and serving. The rapid deployment of LLMs in production environments has driven significant research into efficient inference and serving systems [2, 28–31, 36, 37, 56, 59, 73, 76, 77]. Among them, TensorRT-LLM emphasizes highly optimized CUDA kernels and graph-level optimizations [56]; AlpaServe [37] adopts model parallelism to optimize LLM serving performance; vLLM [36] introducing PagedAttention for dynamic memory management and continuous batching; SGLang [76] advances LLM serving by co-designing the frontend language with the serving backend to enable more efficient execution of complex LLM programs; Splitwise [59] and DistServe [77] explore distributed serving strategies that disaggregate prefill and decoding phases across different resource pools to optimize resource utilization; SarathiServe [2] introduces a chunked prefill approach and piggybacks decoding requests to improve hardware utilization; and HexGen [30] and ThunderServe [29] propose to use heterogeneous resources for cost-efficient LLM serving.

B Illustration of Challenges

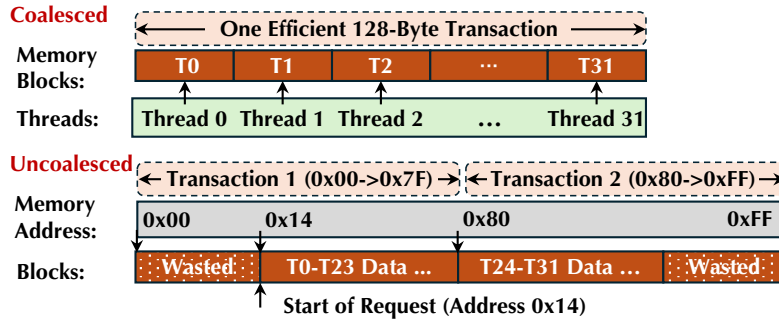


Figure 22. Illustration of wasted memory bandwidth due to uncoalesced memory access (an example of two transactions).

Modern GPUs achieve peak memory bandwidth when the memory addresses accessed by every thread within a warp are within the same aligned segment of global memory (e.g., 3-byte on Hopper/Ampere). This alignment enables the warp to access contiguous memory regions through one efficient global memory transaction [5, 17, 33]. In mixed-precision inference, however, packing weights into low-bit formats results in misalignment between each warp’s memory accesses and the GPU’s standard 32-/64-/128-byte memory segments [53, 54, 70]. This misalignment necessitates multiple global memory transactions per warp for operations rather than one efficient transaction, thereby significantly reducing effective memory bandwidth [18, 34]. As shown in Figure 22.

Shared memory bank conflicts occur when multiple threads within a warp simultaneously access different addresses that map to the same memory bank, forcing these accesses to be serialized rather than executed in parallel, thereby reducing memory throughput by up to an order of magnitude [8, 20, 26, 39]. In mixed-precision inference, low-bit values are typically packed into larger-bit words (e.g., eight INT4 values per 32-bit word [57]) to achieve optimal memory bandwidth and space efficiency [19, 56, 61, 63]. However, packing low-bit weights into larger-bit words makes each column load jump a full packed row (e.g., 128-byte for 32 threads read 32-bit words) [53, 54]. That stride maps every thread in the warp to the same shared memory bank, so the bank must serve the requests one-by-one, turning a parallel-access load into a serialized-access stall, thereby severely degrading memory throughput. As shown in Figure 23.

Modern tensor cores provide INT8/INT4 MMA instructions, but they only run at full throughput when the inputs are pre-packed into fixed tiles (e.g., $16 \times 8 \times 32/64$ for Ampere, $16 \times 8 \times 64/128$ for Hopper) [1, 42]. Standard quantization layouts seldom meet these hardware requirements, creating a fundamental mismatch between them. Consequently, kernels must either inject padding that wastes compute resources, perform costly in-register shuffles at runtime (Figure 24), or fall back to less efficient scalar operations—all of which erode tensor core throughput [19, 38].

C Swizzling

Why swizzling operations are required? Figure 25 illustrates why a swizzled shared memory layout is used in mixed-precision inference. During the prefetch phase, `cp.async` issues horizontal, coalesced row writes to shared memory. During the compute phase, `ldmatrix` performs vertical, per-lane column reads (in groups of eight threads) to feed the tensor cores. With a naïve row-major layout, those vertical reads cause multiple lanes to hit the same shared memory bank, leading to bank conflicts or

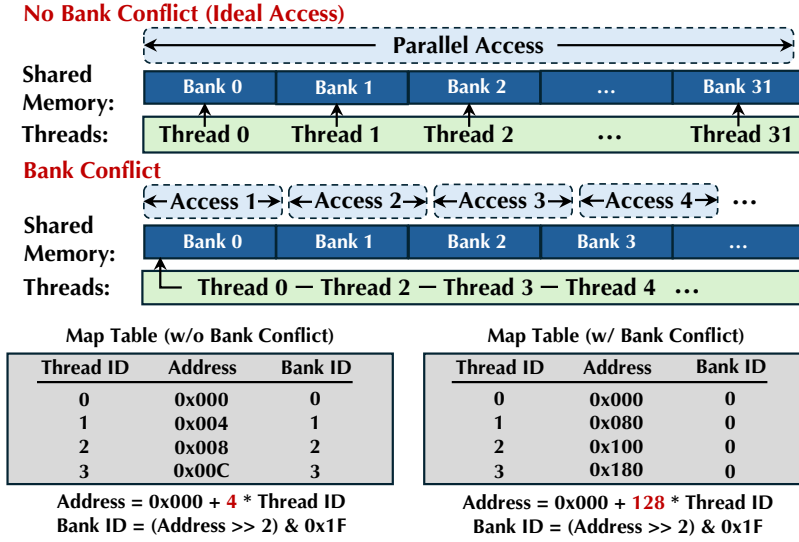


Figure 23. Illustration of reduced memory throughput due to shared memory bank conflicts (an example of 32-way bank conflict).

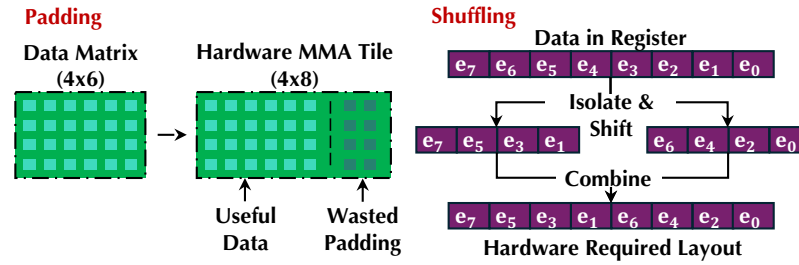


Figure 24. Illustration of padding and shuffling in MMA data misalignment.

extra shuffles. After swizzling, the same logical tile is permuted so that the ldmatrix loads are conflict-free and each lane receives exactly the elements the MMA instruction expects, while the horizontal cp.async writes remain coalesced.

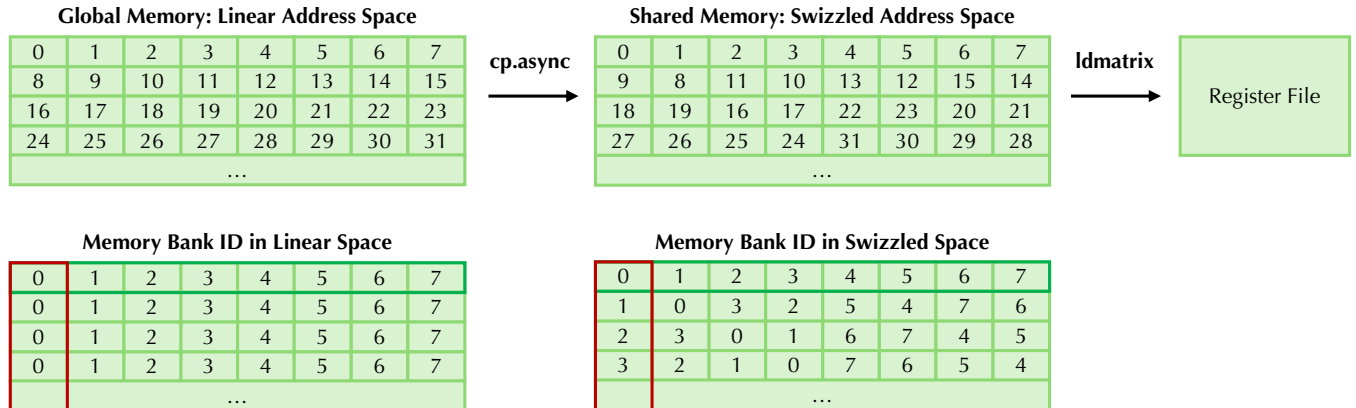


Figure 25. Illustration of 8×128 byte swizzle unit.

Algorithm 1 Q Rearrangement Algorithm

Require: Q_{sm} : Query tile in shared memory, HeadDim: attention head dimension, OP_K: tensor core operand granularity, OP_N: N-dimension operand size, K_N : warp tile size along N dimension, X: batch processing size

Ensure: Register fragment frag_Q in m16n8k16 layout

```
1: /* Thread coordinates within block */
2: lane  $\leftarrow$  lane_id
3: /* Step 1: Compute K-slices based on precision */
4:  $K_K \leftarrow \text{HeadDim}/\text{OP\_K}$ 
5: /* Iterate over N dimension, K-slices with batching */
6: for  $n = 0$  to  $K_N - 1$  do
7:   for  $k = 0$  to  $K_K - 1$  step X do
8:     for  $x = 0$  to  $X - 1$  do
9:       /* Load two fragments at once */
10:      for  $d = 0$  to 1 do
11:        /* Step 2: Coordinate thread mapping to Q */
12:         $hi \leftarrow n \cdot \text{OP\_N} + \lfloor \text{lane}/4 \rfloor$ 
13:         $di \leftarrow k \cdot \text{OP\_K} + (\text{lane} \bmod 4) \cdot 2X + 2x + 8dX$ 
14:        /* Step 3: Load and rearrange Q */
15:         $\text{frag\_Q}[n][k+x][2d] \leftarrow \text{Load}(Q_{sm}[hi][di])$ 
16:      end for
17:    end for
18:  end for
19: end for
20: return frag_Q
```

Why does our packing approach avoid swizzling? Our packing approach packs each logical 16×16 tile into a 32×8 layout; this essentially bakes the swizzle in offline. The 32 rows are just four 8×8 sub-tiles stacked vertically, so when ldmatrix’s 8 participating lanes read columns (vertical), each lane walks its own column and lands on distinct shared memory banks, delivering exactly the fragments tensor cores expect without any runtime shuffles or bank conflicts. Meanwhile, cp.async can still issue horizontal, coalesced row writes because every 32-element row is contiguous in memory.

D Rearrangement Algorithm

Algorithm 1 demonstrates the rearrangement procedure for the m16n8k16 tensor core instruction with a KV head dimension of 128. The variable X is defined as 16 divided by the bit-width of the KV parameter. For example, X equals 2 for an 8-bit KV and 4 for a 4-bit KV.

E Accuracy Evaluation

Table 1. Performance comparison between LMDEPLOY and vLLM using an 8-bit KV cache across various models and datasets.

Model	System	Race-High	GSM8K	MMLU	MMLU-STEM	MMLU-SocSci	MMLU-Hum	Average
Qwen 14B	vLLM	91.05	84.23	87.30	92.36	87.68	83.42	87.67
	LMDEPLOY	90.51	84.38	87.29	92.05	87.83	83.94	87.67
Qwen 8B	vLLM	89.42	76.12	85.24	89.18	86.82	81.31	84.68
	LMDEPLOY	89.17	80.97	85.59	89.93	87.04	81.60	85.72
Llama 8B	vLLM	82.10	80.67	65.82	62.84	68.23	65.12	70.80
	LMDEPLOY	81.68	81.20	71.40	67.05	76.90	72.61	75.14

To verify the correctness of our low-bit KV cache implementation, we demonstrate the accuracy performance comparison between LMDEPLOY and vLLM across three popular models and several existing datasets, as shown in Table 1. The evaluation results demonstrate the accuracy equivalence between the two systems: Both systems achieve highly comparable performance across diverse benchmark tasks, with average score differences consistently remaining within 1-4 percentage points, across

multiple evaluation domains, including reading comprehension, mathematical reasoning, general knowledge assessment, and humanities-specific tasks. This comparison further validates our approach.

F Kernel Benchmarking

Table 2. Performance comparison between LMDEPLOY (INT4×FP16) and cuBLAS (FP16×FP16) GEMM kernels at full utilization on an A100 GPU (problem size: 16384³).

	LMDEPLOY (INT4×FP16)	cuBLAS (FP16×FP16)
Instr. Count	7, 145, 914, 386 (64.66% ↑)	4, 339, 924, 992
Cycle Count	41, 864, 631 (2.89% ↑)	40, 690, 070
Runtime (ms)	30.28 (2.45% ↑)	29.55

As shown in Table 2, We also compare our INT4×FP16 against cuBLAS’s FP16×FP16 GEMM kernel in terms of instruction and cycle counts. The results demonstrate that our kernel requires 64.66% more instructions than cuBLAS’s general kernel, primarily due to the additional dequantization operations. However, this instruction overhead translates to only 2.89% more cycles and 2.45% longer execution time, further demonstrating the effectiveness of our instruction-level parallelism in hiding the dequantization latency.

G Memory Bandwidth Utilization

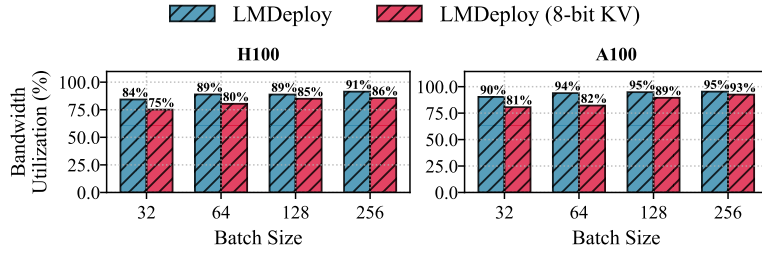


Figure 26. Memory bandwidth utilization of LMDEPLOY’s attention kernel at different batch sizes.

As shown in Figure 26, LMDEPLOY’s attention kernel achieves outstanding memory bandwidth utilization across different batch sizes, reaching up to 91% and 95% with 16-bit KV cache, and achieving a maximum of 86% and 93% with 8-bit KV cache, further proving the effectiveness of our attention pipeline design (§3.4).

H Compare LMDEPLOY with vLLM in General Inference Configuration

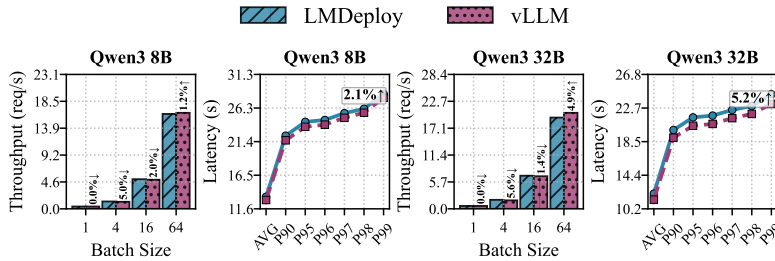


Figure 27. Latency comparison between LMDEPLOY and vLLM using general inference configuration W16A16KV16 (without mixed-precision formats) on H100 GPUs.

As shown in Figure 27, to confirm our performance gains originate from mixed-precision optimization rather than framework differences, we compare LMDEPLOY and vLLM under general inference settings (W16A16KV16). For the Qwen 8B and 32B models, LMDEPLOY performs 8.2% and 4.7% better than vLLM in W4A16KV16 format (Figure 14), whereas LMDEPLOY performs 2.1% and 5.2% worse than vLLM in general format. This contrast further validates the effectiveness of our approach.

I Scalability

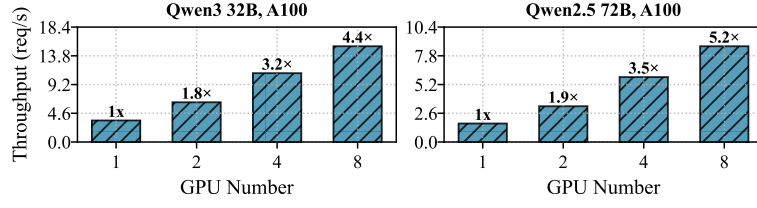


Figure 28. Scalability of LMDEPLOY in multi-GPU serving (tensor parallelism degree = {1, 2, 4, 8}).

Scalability of LMDEPLOY. As shown in Figure 28, we also demonstrate the scalability of LMDEPLOY with increased tensor parallelism degree. For Qwen 32B and Qwen 72B AWQ models, LMDEPLOY scales from 3.44 req/s and 1.68 req/s on a single GPU to 15.3 req/s and 8.7 req/s on 8 GPUs, representing a 4.45 \times and 5.18 \times improvement with 55.6% and 64.8% parallel efficiency, respectively. These results highlight LMDEPLOY’s ability to effectively leverage distributed computing resources for high-throughput LLM serving.